



# Cell Wall Glycans Mediate Recognition of the Dairy Bacterium *Streptococcus thermophilus* by Bacteriophages

Paula Szymczak,<sup>a,b</sup> Sérgio Raposo Filipe,<sup>c,d</sup> Gonçalo Covas,<sup>d</sup>  Finn Kvist Vogensen,<sup>b</sup> Ana Rute Neves,<sup>a</sup> Thomas Janzen<sup>a</sup>

<sup>a</sup>Bacterial Physiology, R&D Microbial Platform, Chr. Hansen A/S, Hørsholm, Denmark

<sup>b</sup>Department of Food Science, University of Copenhagen, Frederiksberg, Denmark

<sup>c</sup>UCIBIO-REQUIMTE, Departamento de Ciências da Vida, Faculdade de Ciências e Tecnologia, Universidade Nova de Lisboa, Caparica, Portugal

<sup>d</sup>Laboratory of Bacterial Cell Surfaces and Pathogenesis, Instituto de Tecnologia Química e Biológica António Xavier, Universidade Nova de Lisboa, Oeiras, Portugal

**ABSTRACT** Receptors on the cell surfaces of bacterial hosts are essential during the infection cycle of bacteriophages. To date, the phage receptors of the industrial relevant dairy starter bacterium *Streptococcus thermophilus* remain elusive. Thus, we set out to identify cell surface structures that are involved in host recognition by dairy streptococcal phages. Five industrial *S. thermophilus* strains sensitive to different phages (*pac* type, *cos* type, and the new type 987), were selected to generate spontaneous bacteriophage-insensitive mutants (BIMs). Of these, approximately 50% were deselected as clustered regularly interspaced short palindromic repeat (CRISPR) mutants, while the other pool was further characterized to identify receptor mutants. On the basis of genome sequencing data, phage resistance in putative receptor mutants was attributed to nucleotide changes in genes encoding glycan biosynthetic pathways. Superresolution structured illumination microscopy was used to visualize the interactions between *S. thermophilus* and its phages. The phages were either regularly distributed along the cells or located at division sites of the cells. The cell wall structures mediating the latter type of phage adherence were further analyzed via phenotypic and biochemical assays. Altogether, our data suggested that phage adsorption to *S. thermophilus* is mediated by glycans associated with the bacterial cell surface. Specifically, the *pac*-type phage CHPC951 adsorbed to polysaccharides anchored to peptidoglycan, while the 987-type phage CHPC926 recognized exocellular polysaccharides associated with the cell surface.

**IMPORTANCE** *Streptococcus thermophilus* is widely used in starter cultures for cheese and yoghurt production. During dairy fermentations, infections of bacteria with bacteriophages result in acidification failures and a lower quality of the final products. An understanding of the molecular factors involved in phage-host interactions, in particular, the phage receptors in dairy bacteria, is a crucial step for developing better strategies to prevent phage infections in dairy plants.

**KEYWORDS** *Streptococcus thermophilus*, bacteriophages, receptors, adsorption, cell wall, polysaccharides, glycans

*Streptococcus thermophilus*, a thermophilic Gram-positive lactic acid bacterium (1), is one of the most common microorganisms used worldwide as a starter in the production of fermented foods, such as cheese and yoghurt (2, 3). The extensive use of *S. thermophilus* in dairy plants results in an increased probability of bacteriophage infections (4). Phage outbreaks represent the major cause of slow or faulty fermentations, frequently leading to a lower quality of dairy products (2, 5).

Diverse treatments have been applied to minimize phage infections in the dairy

Received 27 July 2018 Accepted 14 September 2018

Accepted manuscript posted online 21 September 2018

**Citation** Szymczak P, Filipe SR, Covas G, Vogensen FK, Neves AR, Janzen T. 2018. Cell wall glycans mediate recognition of the dairy bacterium *Streptococcus thermophilus* by bacteriophages. *Appl Environ Microbiol* 84:e01847-18. <https://doi.org/10.1128/AEM.01847-18>.

**Editor** Edward G. Dudley, The Pennsylvania State University

**Copyright** © 2018 Szymczak et al. This is an open-access article distributed under the terms of the [Creative Commons Attribution 4.0 International license](https://creativecommons.org/licenses/by/4.0/).

Address correspondence to Thomas Janzen, [dkthj@chr-hansen.com](mailto:dkthj@chr-hansen.com).

S.R.F. and T.J. contributed equally to this work.

environment. Predominant approaches include chemical and physical methods for equipment sanitation (6) as well as culture replacement and strain rotation programs (7). The latter require strains with identical technological performance but different phage sensitivities (8). This requirement can be met by generating bacteriophage-insensitive mutants (BIMs). The methods to generate BIMs for commercial applications include a secondary culture method (8), serial passage in the presence of high phage titers (9), and chemical mutagenesis (10). Additionally, genetic engineering approaches (11, 12) can be used, in accordance with local legislation. In BIMs of *S. thermophilus*, the mechanisms commonly mediating resistance involve clustered regularly interspaced short palindromic repeat (CRISPR)-Cas systems or restriction-modification (R-M) systems (11, 13, 14), but abortive infection (Abi) (15) and prophage-carried superinfection exclusion (Sie) (16) have less commonly been identified.

CRISPR-Cas and R-M systems target specific genetic sequences of the invading phage (17). These mechanisms have limited robustness, because phages commonly acquire point mutations in their genomes to overcome bacterial immunity (4, 18–21). Additionally, phages acquire methylase genes (22) or produce proteins that inhibit CRISPR-Cas activity (23, 24). Therefore, BIMs in which the resistance is mediated by those mechanisms may not be suitable for industrial applications (3).

To obtain robust phage-resistant variants of *S. thermophilus* strains, strategies to select for BIMs with inhibited phage adherence to the bacterial cell walls were proposed (25). Resistance in these BIMs results from either modification or masking of the phage receptor structure (4, 26). Thus, an understanding of the interactions between the antireceptors of phages and their receptors present on the cell surface of an *S. thermophilus* bacterial strain is a determining factor for the development of phage-resistant cultures.

A knowledge of the structure and properties of bacterial cell walls is advantageous when studying the components recognized by phages. The cell walls of Gram-positive bacteria consist of a peptidoglycan (PG) layer that surrounds the cytoplasmic membrane and is decorated with other glycans and proteins (27). The cell wall glycans comprise two groups of cell surface-associated polysaccharides: (i) exocellular polysaccharides synthesized by the Wzy pathway encoded in the *eps* cluster (free exopolysaccharide [EPS] and capsular polysaccharide [CPS]) (28), and (ii) polysaccharides intercalated with PG (WPS; e.g., pellicles [29] or rhamnose-containing cell wall polysaccharides [30]). A third group of glycans are teichoic acids, classified into wall teichoic acids (WTA), which are covalently bound to PG (31), and lipoteichoic acids (LTA), which are anchored to the membrane (32).

In lactic acid bacteria, the cell wall components involved in the interactions between bacteria and their phages are best studied in *Lactococcus lactis* (3). A correlation between the receptor type present on the cell surface and the tail-tip morphology of the phage has been established (33). Members of two dominating groups of *L. lactis* phages, 936 and P335, which hold complex baseplate structures, recognize specific oligosaccharides of the highly variable pellicle (34–39). *L. lactis* phages from the c2 group have small tail tips (40) and use proteins, either PIP or YjaE, to act as receptors for the irreversible interaction with their hosts (7, 41). In *Lactobacillus delbrueckii*, LTA were designated the receptors for the phage LL-H (42, 43), interacting with a fiber located at the end of the phage tail (44).

To date, four types of *S. thermophilus* phages have been characterized (45–47). The two dominating types, the *cos*- and *pac*-type phages, are genetically distinct but display similar morphological characteristics, possessing long tails (more than 200 nm) with or without fibers on the tail tips (45, 46, 48). Phages belonging to the 5093 type have tails of similar lengths but terminate with globular baseplates (9, 45). The new 987 type comprises phages with short tails (120 to 150 nm) and complex baseplate structures (45, 47).

Phage receptors of *S. thermophilus* may be polysaccharides, teichoic acids, or proteins. Previous studies indicated a role of carbohydrates in the adsorption of phages to *S. thermophilus* (2, 49). Furthermore, the presence of CPS was reported to influence

**TABLE 1** List of *S. thermophilus* strains and phages from the Chr. Hansen A/S collection used in this study

Strain	Characteristic	Dairy production	Sensitive toward phage:	Phage type
STCH_09	Fast-acidifying strain with a texturizing phenotype	Fermented milks	CHPC1057	<i>pac</i>
STCH_12	Fast-acidifying strain	Cheese	CHPC951	<i>pac</i>
STCH_13	Fast-acidifying strain	Cheese	CHPC1014	<i>cos</i>
STCH_14	Fast-acidifying strain	Cheese	CHPC1046	<i>cos</i>
STCH_15	Fast-acidifying strain	Cheese	CHPC926	987

phage sensitivity in *S. thermophilus* (10), while a loss of the ropy phenotype, i.e., the ability to produce exocellular polysaccharides, was associated with the acquisition of phage resistance in a non-CRISPR BIM (14). To date, the identity of phage receptors in *S. thermophilus* remains elusive.

The aim of this study was to identify the phage receptors of *S. thermophilus*. To that end, we generated BIMs of industrial *S. thermophilus* strains and identified mutations putatively involved in phage recognition. Phage-host interactions were visualized via superresolution structured illumination fluorescence microscopy. Biochemical assays were performed to identify the macromolecules recognized by phages with different antireceptor structures. This report establishes the identity of phage receptors at the bacterial cell surface of *S. thermophilus*.

## RESULTS

**Industrial strains and phages selected to unveil phage receptors.** Five industrial *S. thermophilus* strains, representing different lytic groups, and their phages were selected for the study (Table 1). These strains are components of commercial dairy starter cultures and are sensitive to phages that have different antireceptor structures on their tail tips (see Fig. S1 in the supplemental material). Strain STCH\_09 has a texturizing phenotype (free EPS producer) and is infected by phage CHPC1057 (*pac* type), which terminates with a tail fiber. Strains STCH\_12, STCH\_13, STCH\_14, and STCH\_15 are fast-acidifying nontexturizing bacteria that are implemented in processes of cheese fermentation. They are sensitive to phages CHPC951 (*pac* type), CHPC1014 (*cos* type), CHPC1046 (*cos* type), and CHPC926 (987 type), respectively. The first three phages have tail fibers, while the tail of CHPC926 ends with a complex baseplate. The diverse characteristics of these strains and their phages were expected to bring a broad perspective on cell wall structures recognized by *S. thermophilus* phages.

**Putative receptor mutants have mutations in genes encoding glycan biosynthetic pathways.** To identify mutations in genes potentially encoding phage receptors, a range of spontaneous bacteriophage-insensitive mutants (BIMs) was generated from the wild-type (WT) strains by challenging them with their respective phages (Table 1). BIMs of STCH\_09, STCH\_12, STCH\_13, and STCH\_14 were successfully obtained using a plating method, while BIMs of STCH\_15 were generated by growing in liquid medium (see Materials and Methods). The efficiency of BIM formation differed between strains (Table 2).

**TABLE 2** Number of BIMs from five backgrounds generated and selected in this study

Strain	No. of generated BIMs <sup>a</sup>	No. of CRISPR BIMs	No. of sequenced non-CRISPR BIMs
STCH_09	39	13	7
STCH_12	16	6	10
STCH_13	47	31	4
STCH_14	16	10	3
STCH_15	24	7	7

<sup>a</sup>BIMs, bacteriophage-insensitive mutants.

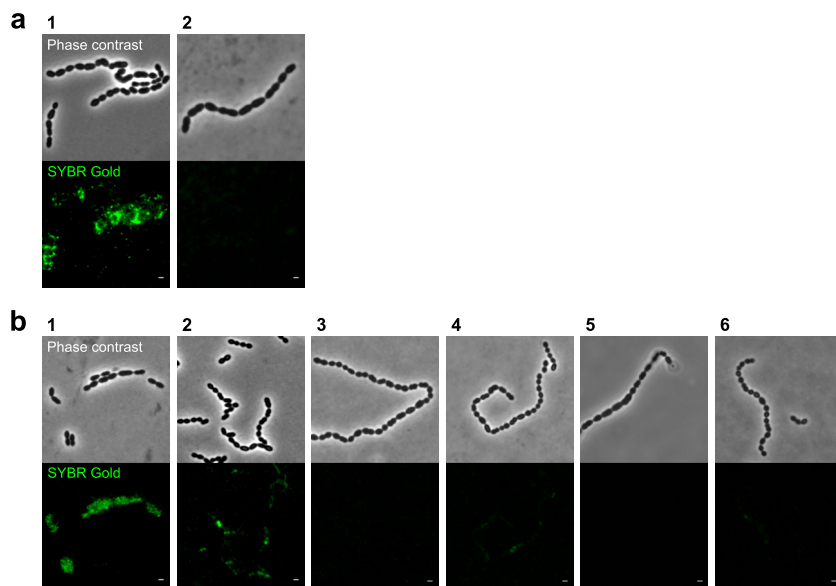


**FIG 1** Changes in phage binding to *S. thermophilus* wild-type strains and their phage-resistant mutants. Phage DNA was labeled with SYBR Gold, and the green fluorescence was visualized. (a) Phage CHPC1057 adsorbs to its host STCH\_09 (panel 1) and does not adsorb to STCH\_09\_BIM (panel 2). (b) Phage CHPC926 adsorbs to its host STCH\_15 (panel 1), has reduced adsorption with STCH\_15\_BIM\_2 (panel 2), and does not adsorb to STCH\_15\_BIM\_1, STCH\_15\_BIM\_3, STCH\_15\_BIM\_4, or STCH\_15\_BIM\_5 (panels 3 to 6, respectively). Scale bars, 1  $\mu$ m.

In this study, we selected for BIMs harboring receptor defects; thus, isolates that became phage resistant due to the activation of a CRISPR-Cas system were excluded. To that end, a colony PCR was performed with primers specific for the CRISPR1, CRISPR2, and CRISPR3 loci in *S. thermophilus* (50). BIMs with spacer acquisitions were visualized on an agarose gel as a product of a larger size compared to that from the WT (data not shown). In total, 67 of 142 tested BIMs were rejected from the investigation as potential CRISPR mutants (Table 2).

The remaining BIMs were subjected to phenotypic assays to select candidates with effective phage resistance and properties of receptor mutants. A spot test was used to assess the reduction of phage titers in non-CRISPR BIMs. The mutants selected for sequencing did not form plaques with their phages, confirming the activation of phage resistance mechanisms independent of CRISPR-Cas systems. An impairment of phage adhesion to non-CRISPR BIMs was examined by mixing BIMs with SYBR Gold-labeled phages and screening them under a fluorescence microscope. BIMs of strains STCH\_09 and STCH\_15 had reduced phage adsorption compared to that of the WTs (Fig. 1). Mutants of strains STCH\_14 and STCH\_15 formed elongated chains compared to those of the WTs, as shown in Fig. S2. These changes in chain lengths are associated with alterations of cell surface properties (27, 30, 31). Changes in the production of free EPS by STCH\_09 and its derivatives were examined with a volumetric pipette viscosity test. Four of seven BIMs of STCH\_09 had altered viscosity compared to that of the WT (see Table S1). On the basis of this characterization, we selected 31 non-CRISPR mutants from the five backgrounds displaying different phenotypic traits (Table 2).

Mutations in genes encoding glycan biosynthetic pathways were detected in the genomes of selected BIMs. The gene modifications are described in Table 3 and Table S2. Briefly, nucleotide substitutions that lead to amino acid substitutions in two glycosyltransferases were detected in STCH\_09\_BIM. The glycosyltransferase *epsH* belongs to the exocellular polysaccharide (*eps*) operon (28), while the other glycosyltransferase belongs to the rhamnose-containing polysaccharide (*rgp*) operon (30). Mutations in genes of *eps* operons were also found in BIMs of fast-acidifying strains STCH\_13, STCH\_14, and STCH\_15. An insertion of three nucleotides in the *epsD* gene of

**TABLE 3** List of mutations in genes encoding glycan biosynthesis pathways detected in BIMs generated in this study

BIM <sup>a</sup>	Mutated gene	Putative gene function	Type of mutation	AA <sup>b</sup> position	Phenotypic change compared to WT
STCH_09_BIM	<i>epsH</i>	Glycosyltransferase	AA substitution	262	Reduced adsorption, enhanced viscosity
	<i>rgp</i>	Glycosyltransferase	Gene truncation	197	
STCH_13_BIM	<i>epsD</i>	Tyrosine-kinase	AA insertion	160	Not detected
STCH_14_BIM	<i>epsE</i>	Priming glycosyltransferase	Gene truncation	37	Long chains
STCH_15_BIM_1	<i>epsE</i>	Priming glycosyltransferase	Gene deletion	Whole gene	Reduced adsorption, long chains
STCH_15_BIM_2	<i>epsK</i>	Glycosyltransferase	AA substitution	75	Reduced adsorption, long chains
STCH_15_BIM_3			Gene truncation	93	Reduced adsorption, long chains
STCH_15_BIM_4			Gene truncation	82	Reduced adsorption, long chains
STCH_15_BIM_5			Gene truncation	93	Reduced adsorption, long chains

<sup>a</sup>BIM, bacteriophage-insensitive mutant.

<sup>b</sup>AA, amino acid.

STCH\_13\_BIM led to the introduction of an additional amino acid in the gene product, while a nucleotide substitution in the *epsE* gene of STCH\_14\_BIM led to gene truncation. A complete deletion of the priming glycosyltransferase *epsE* gene was observed in STCH\_15\_BIM\_1. The four other mutants of STCH\_15 had unique mutations in the glycosyltransferase *epsK* gene, which resulted either in a amino acid substitution, as for STCH\_15\_BIM\_2, or in frameshift and nonsense mutations and ultimately nonfunctional proteins, as for STCH\_15\_BIM\_3, STCH\_15\_BIM\_4, and STCH\_15\_BIM\_5. The BIMs of STCH\_15 had either reduced or lacked phage adsorption as observed under a fluorescence microscope (Fig. 1b). In conclusion, the detected mutations had the potential to affect the production of cell surface-associated polysaccharides, resulting in a loss of phage adherence to some BIMs or, for the BIMs with unchanged phage adsorption, possibly affecting other parameters such as phage DNA injection (14).

**Phage receptors are either located at the septum or distributed uniformly around the cell surface.** With the assumption that cell wall glycans are involved in phage adhesion to *S. thermophilus*, we questioned if phage receptors were located in specific areas on the cell surface and if the location was correlated with the phage antireceptor. Information on phage binding spots might assist in identifying structures recognized by phages, since diverse cell wall structures in Gram-positive bacteria are differently distributed around the cells. For instance, the proteins involved in cell division are located at the septum (51); WTA may locate at the septum or distribute irregularly in mature PG (52–54), while cell surface-associated polysaccharides evenly surround the cells (29, 55). To specify the receptor locations on the cell surface, phage-host interactions were visualized via conventional and superresolution fluorescence microscopy.

Two distinct patterns of phage adhesion to the host cells were observed via microscopy techniques. Phage particles, for which their DNA was labeled with SYBR Gold, were either irregularly distributed throughout the cell surface or created a dispersed halo that surrounded the host cells when visualized with a conventional fluorescence microscope (Fig. 2a). The spotty and diffused binding patterns were additionally verified by using superresolution structured illumination microscopy (SR-SIM) (Fig. 2b and S3). The fluorescent signals of phages CHPC926, CHPC951, and CHPC1057 were localized at division sites of the host cells: at the septum, in the areas where a septal membrane ring began to build, or where the cell wall has been produced and split (Fig. 2b, panels 1 to 3). *cos*-type phages CHPC1014 and CHPC1046, which hold fibers at the ends of their tails, displayed dispersed fluorescent signals distributed uniformly along the cells (Fig. 2b, panels 4 and 5). The type of binding did not depend on the ratio of phages toward their hosts. The test was performed at multiplicities of infection (MOI) of approximately 10 and 1, and differences between the two conditions were not observed; i.e., the nature of adsorption, spotty or diffused, remained unaffected (data not shown). Furthermore, the distance between a phage capsid, which contained DNA labeled with a green fluorophore (SYBR Gold), and a bacterial membrane stained with a red fluorophore (Nile red) is in accordance with the values determined by electron microscopy for the length of the phage tails and

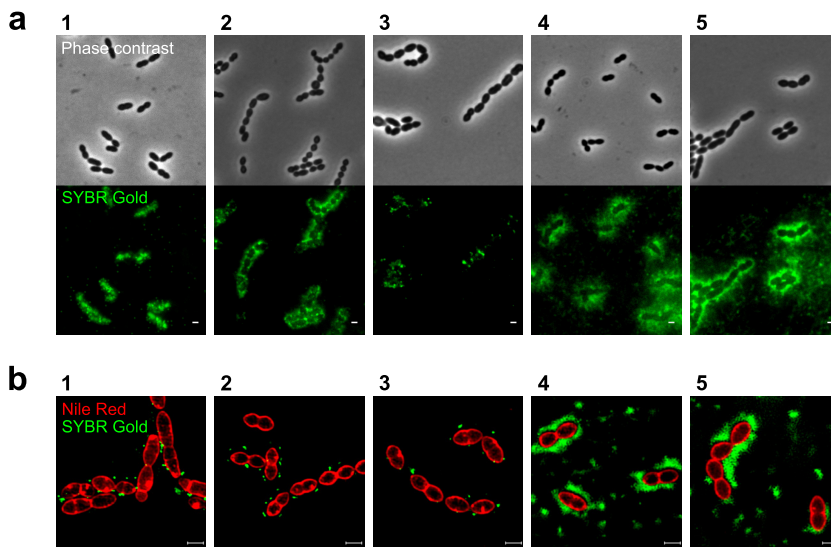


**FIG 2** Fluorescence imaging of phage binding to *S. thermophilus* strains. (a) Adsorption of phages to their hosts was visualized with a conventional fluorescence microscope after labeling phage DNA with SYBR Gold. (b) Superresolution structured illumination microscopy (SR-SIM) images of bacterial cells stained with Nile red (red) and mixed with SYBR Gold DNA-labeled phages (green). Panels with phages and their host strains: 1, CHPC926 and STCH\_15; 2, CHPC951 and STCH\_12; 3, CHPC1057 and STCH\_09; 4, CHPC1014 and STCH\_13; 5, CHPC1046 and STCH\_14. Two binding patterns are observed: spotty (panel numbers 1, 2, and 3) or diffused (panel numbers 4 and 5). Scale bars, 1  $\mu\text{m}$ .

provided additional evidence that the green fluorescence signal represents phage binding (Fig. 3).

**Binding of a phage at the septum is mediated by cell wall glycans.** We wanted to identify which cell wall components were involved in the phage adsorption at the septal areas of the cells, because we commonly observed this type of phage-host interaction in *S. thermophilus* and we detected spotty adsorption with phages having

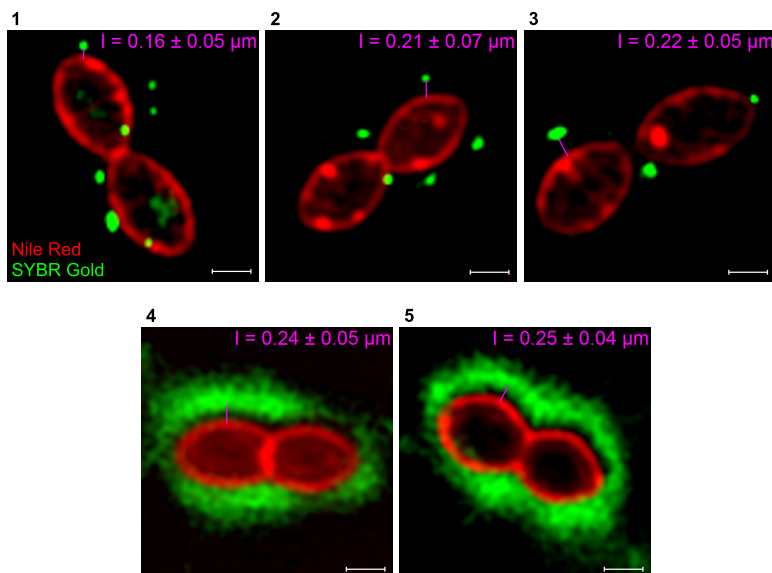


**FIG 3** Superresolution structured illumination microscopy (SR-SIM) images of phage binding to *S. thermophilus* strains. The pink lines indicate the distance between phage capsids, containing SYBR Gold-labeled DNA (green), and bacterial membranes, stained with Nile red (red). The presented values correspond to the lengths of phage tails and are the averages from 80 measurements. Panels with phages and their host strains: 1, CHPC926 and STCH\_15; 2, CHPC951 and STCH\_12; 3, CHPC1057 and STCH\_09; 4, CHPC1014 and STCH\_13; 5, CHPC1046 and STCH\_14. Scale bars, 0.5  $\mu\text{m}$ .

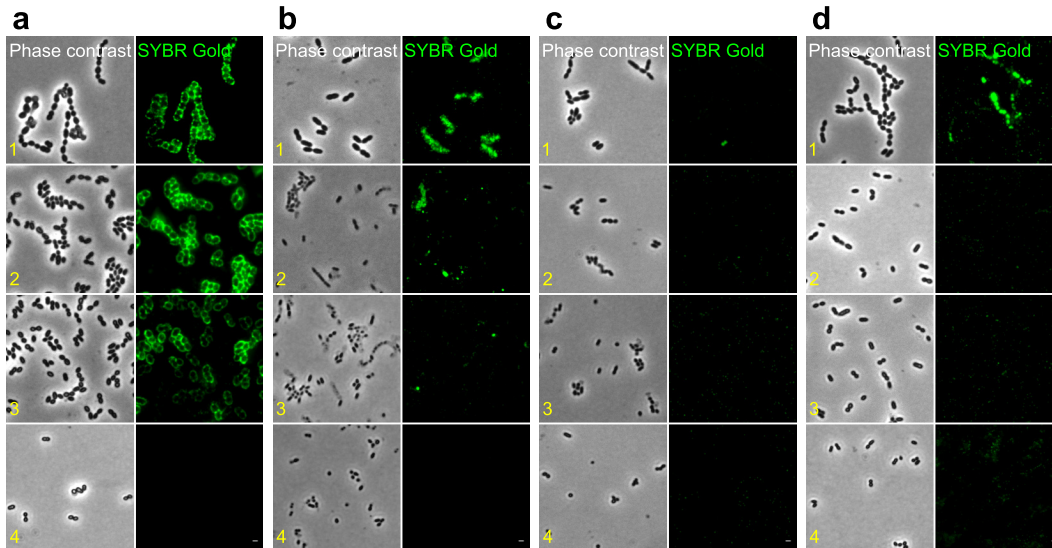


**FIG 4** Fluorescence imaging of phage binding to cellular fractions of *S. thermophilus*. Phage DNA was labeled with SYBR Gold and the green fluorescence was visualized. (a) Phage CHPC951 was mixed with cellular fractions of STCH\_12. Phage CHPC926 was mixed with cellular fractions of STCH\_15 (b), cellular fractions of STCH\_15\_BIM\_1 (c), or cellular fractions of STCH\_15\_BIM\_2 (d). The following samples were used: 1, cells in exponential phase; 2, cells devoid of surface enzymes, membranes, and membrane proteins; 3, purified cell walls; 4, purified peptidoglycan. Scale bars, 1  $\mu\text{m}$ .

different tail-tip morphologies. Thus, two strains with phage receptors located at the septa were selected for further study: STCH\_12, infected by *pac*-type phage CHPC951 with a tail fiber, and STCH\_15, infected by 987-type phage CHPC926 with a baseplate. Additionally, to verify the effects of mutations of *eps* genes on phage receptors, STCH\_15\_BIM\_1 and STCH\_15\_BIM\_2 were used in the assays.

To assess the involvement of different cell wall components in phage recognition, the selected *S. thermophilus* strains were treated as described in Materials and Methods (see Table S3) to deplete sequentially cellular components: (i) surface enzymes, membrane, and membrane proteins (purification step no. 2), (ii) LTA and cell wall proteins (purification step no. 3), (iii) WTA, WPS, and CPS (purification step no. 4). We assumed that exocellular polysaccharides loosely associated with the cell surface detached gradually in the multiple centrifuging steps applied in the preparation of cellular fractions. Subsequently, phage binding to the isolated cellular fractions was verified under a fluorescence microscope.

Phages with different antireceptor structures attached to different cellular fractions of their hosts. Phage CHPC951 adsorbed to the surface of strain STCH\_12 until purification step no. 4 was applied (Fig. 4a, panel 4). The adsorption of phage CHPC926 to the surface of strain STCH\_15 was gradually reduced after purification steps no. 2 and 3 (Fig. 4b, panels 2 and 3, respectively). Thus, phage CHPC951 with a tail fiber established a binding complex with one of the cell wall glycans but not with PG. Phage CHPC926 with a baseplate interacted either with cell wall proteins, LTA, or exocellular polysaccharides associated with the cell surface.

Exocellular polysaccharides were the most probable phage receptors of STCH\_15, since its BIMs held mutations in genes belonging to the *eps* operon. However, the production of extracellular matrix masking phage receptors might be another consequence of mutations of *eps* genes. Phage CHPC926 did not adsorb to any of the cellular fractions of STCH\_15\_BIM\_1 (Fig. 4c), which indicated a substantial modification or even a deletion of a phage receptor. For STCH\_15\_BIM\_2, phage adsorption was observed only with the cells in exponential phase (Fig. 4d, panel 1), which suggested that the phage bound to modified exocellular polysaccharides until these were depleted in subsequent purification steps.

The effect of *eps* genes mutations on CPS formation was further assessed by the India ink negative staining method (Fig. 5). STCH\_15 possessed CPS, visible as a

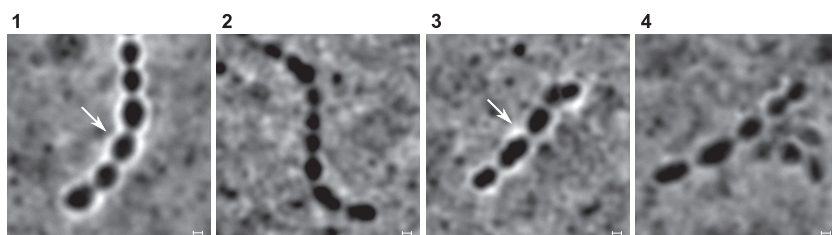


**FIG 5** Microscopy images of India ink negatively stained *S. thermophilus* strains. Staining was performed for two wild-type strains and two phage-resistant mutants: 1, STCH\_15; 2, STCH\_15\_BIM\_1; 3, STCH\_15\_BIM\_2; 4, STCH\_12. Presence of capsular polysaccharide is indicated with arrows. Scale bars, 1  $\mu\text{m}$ .

transparent halo surrounding the cells (Fig. 5, panel 1). STCH\_15\_BIM\_1, which was proposed to have phage receptor deletion, completely lacked CPS, because a transparent halo engulfing the cells was not detected (Fig. 5, panel 2). STCH\_15\_BIM\_2 produced less CPS, as indicated by the less clear halo (Fig. 5, panel 3). On the basis of the observations made for the two BIMs, the mutations in genes belonging to the *eps* operon in STCH\_15 caused modifications in exocellular polysaccharides which act as the phage receptor for the CHPC926 phage with a baseplate.

Macromolecules such as WTA, WPS, or CPS might mediate the adsorption of phage CHPC951 with a tail fiber. Thus, we evaluated the host potential to synthesize these molecules by searching for genes encoding their biosynthetic pathways in the genome. All *S. thermophilus* strains possessed two polysaccharide gene clusters: the *eps* operon (28) and the *rgp* operon (30). However, analogs of the *tag* and *tar* genes essential for WTA synthesis were missing; thus, WTA were excluded as receptors (31). In addition, STCH\_12 showed no halo in response in the India ink staining test, indicating very low production or absence of CPS (Fig. 5, panel 4). Thus, it is reasonable to propose that the putative receptors for fiber-ending phage CHPC951 are polysaccharides intercalated with PG, most likely WPS encoded by the *rgp* operon.

The PG was excluded as a phage receptor in *S. thermophilus*, since none of the phages were found to bind the purified PG (Fig. 4a to d, no. 4 panels). The PG compositions of *S. thermophilus* progenitors and mutants were identical, as determined by the high-pressure liquid chromatography (HPLC) profiles due to the amount and type of muropeptides released with PG that was incubated with PG hydrolase (see Fig. S4). Moreover, the monosaccharides present in the glycan chain, *N*-acetylglucosamine and *N*-acetylmuramic acid, were identified in the PG at the same relative concentrations for the WTs and BIMs (see Fig. S5a). Thus, PG did not seem to be the structure recognized by *S. thermophilus* phages.

#### **Composition of saccharides in glycan chains is crucial for phage adsorption.**

Cell wall glycans commonly differ in linkage, branching, and substitutions (28, 30, 56). We questioned if the specific composition of saccharides in chains was necessary for the efficient binding of the phages. To that end, the monosaccharide compositions were analyzed in samples collected during the purification of cellular fractions of WTs and BIMs (Table S3). Although the cell walls of WTs and BIMs were composed of the same monosaccharide types, the ratios of carbohydrates varied between the strains. The cellular fractions of *S. thermophilus* strains were composed of monosaccharides typical for the PG structure, *N*-acetylglucosamine and *N*-acetylmuramic acid, as well as rhamnose, galactose, and glucose. However, STCH\_12 had the largest amount of glucosamine and the smallest amount of glucose among all the strains, while STCH\_15 had less glucosamine and more glucose than its BIMs (Fig. 6; Fig. S5b). The calculation was based on the profiles generated for purified cell walls with polysaccharides anchored to PG (WPS and CPS). The differences in monosaccharide profiles of the cell walls indicated that WTs and BIMs had unique glycan compositions that were linked to the differences in phage sensitivities.

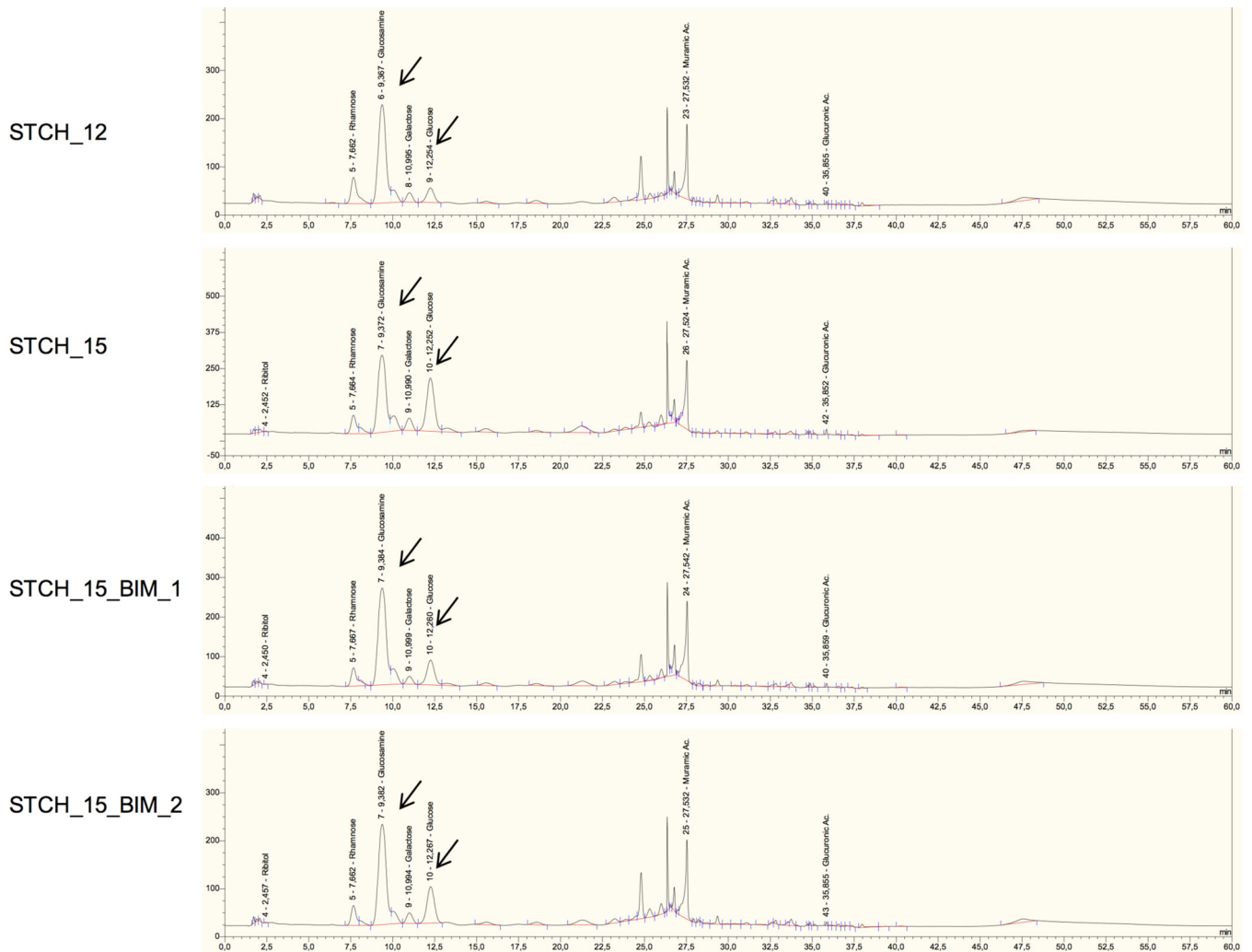


**FIG 6** Profiles of monosaccharide compositions in purified cell walls isolated from *S. thermophilus* strains. HPAEC-PAD analyses were performed for cell walls purified from two wild-type strains (STCH\_12 and STCH\_15) and two phage-resistant mutants (STCH\_15\_BIM\_1 and STCH\_15\_BIM\_2). Standards for different saccharides were eluted under the same conditions to enable peak identification. Differences in the heights of glucosamine and glucose peaks are indicated with arrows.

## DISCUSSION

In this work, we obtained evidence supporting the involvement of cell wall glycans on phage adsorption to dairy strains of *S. thermophilus*. The macromolecular receptors are either regularly distributed along the cells (dispersed pattern) or located at septal areas of the cells (spotty pattern). The spotty pattern of adherence is mediated by different cell wall components: the fiber-ending phage CHPC951 adsorbs to polysaccharides anchored to PG, while the baseplate phage CHPC926 binds to exocellular polysaccharides associated with the cell surface. On the basis of the results from a combination of genetic and biochemical approaches, we propose that Wzy-dependent exocellular polysaccharides and WPS are phage receptors in *S. thermophilus*.

In BIMs of *S. thermophilus*, the recurrence of mutations in genes involved in glycan biosynthetic pathways, e.g., those encoding glycosyltransferases, the priming glycosyltransferase, and the bacterial tyrosine-kinase, strongly indicates a role of cell surface glycans in the phage-host interaction. This view is in line with an observed loss of phage adsorption to several of these BIMs. Previously, free EPS contributing to a ropy phenotype was reported to be related to phage sensitivity in *S. thermophilus* (14). The results of our study show that *S. thermophilus* acquires mutations in genes of the *eps* operon (biosynthesis of free EPS and CPS) as a response to phage infections, indepen-

dent of a texturizing phenotype. Moreover, mutations in glycan biosynthetic pathways genes occurred in response to phages of different types, including the dominating *pac*- and *cos*-type phages with tail fibers as well as 987-type phages with baseplate at the tail tips. With a consideration of these findings, one may speculate that in *S. thermophilus*, cell wall glycans are universal receptors for phages.

Approximately 50% of the BIMs generated by challenging *S. thermophilus* with their phages were CRISPR mutants, a result that was not surprising considering that the activation of intracellular defense strategies is the predominant response to phage attack (3, 14). Mutations in R-M systems were rare in the fraction of non-CRISPR BIMs. Of these, circa 25% carried mutations in glycan biosynthesis genes. The impact of these mutations on the performance of the strains needs to be evaluated prior to industrial use. Moreover, to link these mutations with the reduced phage sensitivity and loss of adsorption, the inactivation of the target gene in the mother strain or the restoration of the phenotype by the introduction in *trans* of the wild-type gene can be envisioned. Although these genetic approaches commonly applied to domesticated strains might be appealing, they are difficult to implement in industrial strains that are not genetically amenable and for which tools for genetic manipulation are largely unavailable (57). We assumed that the complementation of gene mutations in the studied strains would be challenging. Therefore, we resorted to phenotypic and biochemical approaches to further substantiate our hypothesis that cell wall glycans act as phage receptors in *S. thermophilus*.

The common *S. thermophilus* *pac*- and *cos*-type phages with tail fibers (e.g., CHPC951) likely bind to polysaccharides anchored to cell walls. This observation conflicts with the previous idea that phages with simple antireceptors bind to conserved structures with repetitive units, such as proteins or teichoic acids (3, 33). The *S. thermophilus* strains used in this study contain in their genome sequences two operons involved in glycan biosynthesis pathways, namely, the *eps* operon encoding the biosynthetic pathway for the synthesis of free EPS and/or CPS and the *rgp* operon for the synthesis of WPS intercalated with PG. The absence of genes required for the synthesis of WTA is in agreement with the view that *S. thermophilus* does not synthesize WTA (30, 58), ruling out this macromolecule as a possible phage receptor. Furthermore, adsorption assays with purified cellular fractions enabled the exclusion of proteins, LTA, and purified PG as phage receptors for the strain infected by the fiber-ending phage. In this line of reasoning, we singled out polysaccharides anchored to PG as the only surface glycans that could interact with phage CHPC951.

Our results suggest that phages with baseplates (e.g., CHPC926) recognize CPS on the cell surface. Indeed, the spatial arrangement of baseplates is required to bind complex structures of heteropolysaccharides, such as those produced by the Wzy pathway (free EPS and CPS) or WPS (3, 33). In line with this, cell wall-associated polysaccharides in *L. lactis* are recognized by phages from the group P335 (34, 36, 38, 59), which are genetically related to 987-type *S. thermophilus* phage CHPC926 (45). Although proteins could be a secondary factor that mediates efficient binding, as in the case of *L. lactis* phages from the group c2 (7, 41), mutations in genes coding for putative membrane proteins were not found in sequenced BIMs, and thus proteins are unlikely required for phage-host interactions in *S. thermophilus*. Mutations in *eps* genes resulted in the production of an altered polysaccharide in the BIMs, as denoted by the monosaccharide composition, which correlated with the absence or reduction of phage adherence to the cellular fractions of the BIMs. As for the WT, phage binding was not detected in purified cell walls with intercalated WPS. Altogether, exocellular polysaccharides associated with cell walls (most likely CPS) are the structures mediating the adsorption of phage CHPC926 with a baseplate.

The type of adsorption, spotty or dispersed, and the phage tail-tip morphology were not correlated. Phage adsorption at the septal areas of the cells (spotty pattern) was observed for the phage with a baseplate as well as *pac*-type phages with tail fibers, while dispersed adsorption was observed for two *cos*-type phages with tail fibers. The two adsorption patterns might indicate that different types of *S. thermophilus* phages

recognize distinct cell wall structures, that the same macromolecule displays different conformation/folding depending on location, or that the locations of the recognized macromolecules on the cell surface differ between *S. thermophilus* strains. The latter alternative seems more plausible, as substantiated below. *S. thermophilus* strain STCH\_12 is sensitive to a number of *cos*- and *pac*-type phages with fiber-ending tails. Interestingly, a spotty pattern of adsorption to this strain was observed with all infective phages, independently of their type (data not shown). Thus, the macromolecule/structure recognized by phages of STCH\_12 was located at the septum, supporting the view that the location of the receptor macromolecule is strain dependent. In summary, as with phages with a baseplate, fiber-ending phages also recognize cell surface glycans, namely, exocellular polysaccharides.

On the basis of our fluorescence microscopy results on adsorption patterns, polysaccharides can be either located at the septum or distributed evenly on the cell surface. The underlying mechanisms behind this phenomenon need to be investigated. However, the differential location of cell wall glycans at the surfaces of Gram-positive bacteria has been documented. In *Bacillus subtilis*, WTA are only detected at the septum (52), while in *Staphylococcus aureus*, they either are associated with the mature PG (54) or have two forms, one located at the septum and another distributed throughout the cell (53).

However, with the knowledge that antireceptor structures of *cos*- and *pac*-type phages are different, we cannot exclude that the two adsorption patterns indicate that different receptors are recognized. Fibers at the end of the tail are expected to mediate the primary interaction with macromolecules on the cell surface, while more distant tail-tip structures might be necessary for the efficient binding and phage DNA injection, similar to the model of interaction proposed for *Lactobacillus delbrueckii* and its phage LL-H (44). Since morphological differences might not be visible under the electron microscope, more information on the phage structures involved in host recognition is necessary for understanding the difference in adsorption patterns of phages with outwardly identical tail fibers.

In this study, SR-SIM was used to track phage-host interactions. This novel application is advantageous over standard methods for testing phage adsorption, such as conventional fluorescence microscopy, because the high resolution enables a more detailed view of phage binding spots. The combination of superresolution microscopy techniques with the understanding of the complex nature of the cell wall dynamics and structures of phage antireceptors is expected to add value for exploring phage-host interactions.

In conclusion, the results of this study provide evidence that exocellular polysaccharides and WPS are involved in phage adsorption in *S. thermophilus*. The identification of phage receptors of *S. thermophilus* will contribute to future strategies aimed to design robust phage-resistant dairy starter cultures.

## MATERIALS AND METHODS

**Bacteria, phages, and growth conditions.** The *Streptococcus thermophilus* strains and phages used for this study are listed in Table 1. The strains were stored at  $-40^{\circ}\text{C}$  in growth medium supplemented with 15% (wt/vol) glycerol and cultured overnight at  $37^{\circ}\text{C}$  in LM17 broth (M17 broth [Oxoid, Denmark] with 2% [wt/vol] lactose) or anaerobically at  $37^{\circ}\text{C}$  on LM17 agar plates (M17 agar [Oxoid] with 2% [wt/vol] lactose). For the bacterial cells used for tests with phages, the growth medium was additionally supplemented with 10 mM  $\text{CaCl}_2$  and 10 mM  $\text{MgCl}_2$  (LM17-Ca/Mg). *Streptococcus pneumoniae* strain Pen6 (60), which was used as a control for the procedure of subtracting cellular components, was stored at  $-80^{\circ}\text{C}$  in growth medium supplemented with 15% (wt/vol) glycerol and cultured in a casein-based semisynthetic medium (C+Y) at  $37^{\circ}\text{C}$  as described previously (61).

The phages were propagated as previously described (45) and stored at  $4^{\circ}\text{C}$ . Phage titers as well as the host ranges of investigated phages with bacterial strains were determined with the double agar overlay spot test, as described previously (62). After an overnight incubation under the appropriate growth conditions, the PFU per milliliter was calculated.

Bacteriophage-insensitive mutants (BIMs) were formed via two methods. The plating method was adapted from a published protocol (9), where an overnight culture of a sensitive host was mixed with adequate phages at a multiplicity of infection (MOI) of  $\geq 1$  (ratio of PFU to CFU per milliliter), plated in soft top agar (LM17-Ca/Mg broth and agar mixed 1:1), and monitored for the appearance of phage-resistant colonies after 24 to 48 h of incubation under the growth conditions. If no colonies grew, the MOI

was reduced by mixing the bacteria with a diluted phage lysate, and the procedure was repeated. To increase the probability that the generated BIMs would acquire unique mutations, several single colonies of each wild-type (WT) strain were inoculated in individual tubes and plated on separate plates after mixing with adequate phages. Due to the inefficient lysis with one of the phages used in the study, the secondary culture method was performed (8), where LM17-Ca/Mg broth was inoculated with a 1% overnight culture of a sensitive host, followed by the addition of adequate phages at an MOI of 10 or an MOI of 0.01 and incubating at 37°C. Surviving cells were collected at two time points, after 5 h and after 72 h of incubation, centrifuged at  $15,000 \times g$  for 10 min, resuspended in saline, mixed with adequate phages at an MOI of  $\geq 1$ , plated in soft top agar, and monitored for the appearance of phage-resistant colonies after an overnight incubation under the growth conditions. BIMs generated in both assays were purified by streaking on LM17 agar plates and incubating under the growth conditions in three sequential repetitions.

**Volumetric pipette viscosity test.** To test for differences in the production of exocellular polysaccharides (free EPS) between the strain with texturizing phenotype and its BIMs, 250 ml of boiled milk was inoculated with 1% overnight cultures and incubated overnight at 37°C. The samples were cooled to room temperature, gently mixed, and pipetted with a 25-ml pipette. The time for an unforced flow through the pipette was measured in three repetitions. The thresholds for viscosity changes were as follows: 25 to 34 s (reduced viscosity), 35 to 44 s (normal viscosity), and 45 to 54 s (increased viscosity).

**Microscopy techniques.** Microscopy screening of overnight cultures was performed to detect changes in cell chain lengths between WTs and BIMs. The cells were immobilized on a thin layer of 1% agarose in PreC medium (63). Photographs were taken using a Zeiss Axioplan 2 microscope equipped with a Plan-Neofluar objective (100 $\times$ , 1.3 oil, Ph3) and a Zeiss Axiocam 503 monocular camera (Zeiss, Germany).

The presence of CPS was tested via the India ink negative staining technique (55) with the modification that a mix of 7  $\mu$ l of India ink with 7  $\mu$ l of fresh milk and 3  $\mu$ l of bacterial sample was prepared on a microscopy slide. After air-drying, the samples were visualized under the Zeiss Axioplan 2 microscope, with the specifications described above. After acquisition, the photos were processed with ZEN software (black edition, version 14.0.0.201).

Changes in phage adsorption to the bacterial cell walls before and after the depletion of cellular components were visualized under a fluorescence microscope. Freshly propagated phages were mixed 1,000:1 (vol/vol) with a 10-fold-diluted SYBR Gold stock solution (Invitrogen, USA) and incubated overnight in the dark at 4°C (45, 64). Bacterial cultures at exponential phase (optical density at 600 nm [OD<sub>600</sub>] of 0.5) and samples obtained during the purification of cellular fractions in steps no. 1 to 4 (see Table S3 in the supplemental material) were mixed with stained phages at MOIs of approximately 10 and 1 in LM17-Ca/Mg. The mixtures were immobilized on a thin layer of 1% agarose in PreC medium as described above. Photographs were taken with a 1-s exposure by using a Zeiss Axio Observer microscope with a Plan-Apochromat objective (100 $\times$ , 1.4 oil, Ph3). Images were acquired with a Retiga R1 charge-coupled-device (CCD) camera (QImaging, Canada) and Metamorph 7.5 software (Molecular Devices, USA). After acquisition, the images were processed with ImageJ software (65).

Phage binding patterns were visualized by superresolution structured illumination microscopy (SR-SIM) because of its improved resolution compared to that of conventional microscopy (66). Bacterial cultures at exponential phase (OD<sub>600</sub> of 0.5) were stained with 2  $\mu$ l/ml Nile red (Invitrogen), incubated for 5 min at room temperature with agitation in the dark, and washed twice with LM17-Ca/Mg. Membrane-stained bacterial cells were mixed with SYBR Gold-labeled phages (MOI  $\geq 10$ ) and mounted on a 1% PreC agarose pad as specified above. Imaging was performed on an Elyra PS.1 microscope (Zeiss) with a 561-nm laser at 50% power and a 50-ms exposure for Nile red and a 488-nm laser at 20% power and a 50-ms exposure for SYBR Gold. The images were acquired via five grid rotations, with a 34-mm grating period for the 561-nm laser and a 28-mm grating period for the 488-nm laser, followed by the reconstruction and processing with ZEN software (black edition, version 14.0.0.201).

Transmission electron micrograph images of phages were generated according to the method described previously (45).

**Depletion of cellular components.** The purification of cellular fractions was performed via the previously described method (67), with a modification that overnight cultures were subcultured into 2 liters of LM17 broth (for *S. thermophilus*) or 2 liters of C+Y medium (for *S. pneumoniae*) at an initial OD<sub>600</sub> of 0.01 and grown until the OD<sub>600</sub> was between 0.5 and 1.0 (step no. 1). Chemical and enzymatic treatments were applied to the bacterial cell walls to progressively remove different cell wall components. Briefly, the cells were boiled with sodium dodecyl sulfate (SDS) and then washed with Milli-Q water to obtain cells devoid of surface proteins and membranes (step no. 2). The sample was considered devoid of exocellular polysaccharides loosely associated with the cell surface, as they detached during the multiple centrifugations applied in this step. The subsequent treatment with enzymes, lithium chloride (LiCl), EDTA, and acetone was executed to remove components ionically bound to the cell wall, such as proteins, as well as LTA and intracellular components, i.e., DNA and RNA (step no. 3). The obtained cell walls with WTA, WPS, and CPS were treated with 46% hydrofluoric acid (HF) according to the previously described protocol (67) and incubated at 4°C for 72 h (step no. 4). In this step, cell surface glycans were separated from PG. Aliquots of the cellular fractions (Table S3) were stored at -20°C until further analyses were performed.

The monosaccharide compositions in samples collected during the purification of cellular fractions (Table S3) were examined by high-performance anion-exchange chromatography coupled with pulsed amperometric detection (HPAEC-PAD) as described previously (67). The volumes of samples used for hydrolysis with hydrochloric acid (HCl) prior to the injection in the column were

100  $\mu$ l for cells collected at exponential phase, 40  $\mu$ l for cells devoid of surface enzymes, membranes, and membrane proteins (this amount corresponded to approximately  $1 \times 10^9$  cell equivalents), 20  $\mu$ l at a concentration of 40 mg/ml for purified cell walls, and 20  $\mu$ l at a concentration of 20 mg/ml for purified PG. The standards for monosaccharides typically present in cell walls of Gram-positive bacteria (glucosamine, *N*-acetylglucosamine, muramic acid, *N*-acetylmuramic acid, rhamnose, glucose, galactose, ribitol, fucose, ribose, mannose, and glucuronic acid [28, 56]) were eluted under the same conditions to enable the identification of chromatogram peaks.

Muropeptides present in purified PG were prepared and analyzed by reverse phase HPLC as previously described (67).

**Molecular techniques.** To exclude BIMs that acquired phage resistance due to the activation of a CRISPR-Cas system, a colony PCR was performed with primers specific for three CRISPR loci in *S. thermophilus* (50). The PCRs were prepared using PCR master mix (Roche, Germany) with the following conditions: 94°C for 2 min, followed by 30 cycles of 94°C for 45 s, either 48°C (CR2 and CR3) or 51°C (CR1) for 45s, and 72°C for 2 min, with a final extension of 72°C for 5 min. The PCR products were visualized on a 1% tris-acetate-EDTA (TAE) agarose gel.

To perform full genome sequencing, DNA from the selected *S. thermophilus* strains was isolated by using the DNA DNeasy blood and tissue kit with the protocol for Gram-positive bacteria (Qiagen, Germany) and sent for sequencing on the Illumina MiSeq platform with  $2 \times 250$ -bp paired-end sequencing (Illumina, USA).

Sequencing reads were trimmed, analyzed, and assembled with the CLC Genomics Workbench 10.1.1 (Invitrogen). The assembled contigs were annotated by RASTtk (68). Single nucleotide polymorphism (SNP) analyses of WT and BIMs were performed with CLC Genomics Workbench 10.1.1 (Invitrogen). The detected mutations were further evaluated to exclude false hits, i.e., SNPs at the ends of contigs, SNPs in noncoding regions not related to a putative promoter or a putative terminator, SNPs at mobile element proteins, and SNPs not resulting in amino acids changes. The analysis was performed by using CLC Main Workbench 7.7.3 (Invitrogen). The revised mutations were additionally verified by PCR, followed by Sanger sequencing (Macrogen, The Netherlands).

**Accession number(s).** The gene sequences reported in Table 3 together with the corresponding gene sequences in the WT strains are available in GenBank under the accession numbers [MH700463](https://doi.org/10.1128/MH700463) to [MH700476](https://doi.org/10.1128/MH700476).

## SUPPLEMENTAL MATERIAL

Supplemental material for this article may be found at <https://doi.org/10.1128/AEM.01847-18>.

**SUPPLEMENTAL FILE 1**, PDF file, 1.2 MB.

## ACKNOWLEDGMENTS

We thank Mimi Birkelund, Ditte E. Christiansen, Martin H. Rau, and João M. Monteiro for their help collecting data and the other colleagues from Chr. Hansen A/S and ITQB-NOVA for valuable discussions. We thank Mariana G. Pinho for providing access to the superresolution structured illumination microscope at ITQB-NOVA (Oeiras, Portugal). We also thank Horst Neve from Max Rubner-Institut (Kiel, Germany) for providing the electron micrograph images of phages.

This work is part of an Industrial PhD project funded by Innovation Fund Denmark and Chr. Hansen A/S, grant no. 4135-00104B.

P.S. collected and analyzed the data and prepared a draft of the paper, T.J. and S.R.F. designed the experiments and evaluated the data, G.C. collected the data, and F.K.V. and A.R.N. evaluated the data. All authors reviewed the manuscript.

## REFERENCES

- Lahtinen S, Ouwehand AC, Salminen S, Von Wright A. 2012. Lactic acid bacteria: microbiological and functional aspects, 4th ed. CRC Press, Boca Raton, FL.
- Binetti AG, Quiberoni A, Reinheimer JA. 2002. Phage adsorption to *Streptococcus thermophilus*. Influence of environmental factors and characterization of cell-receptors. *Food Res Int* 35:73–83. [https://doi.org/10.1016/S0963-9969\(01\)00121-1](https://doi.org/10.1016/S0963-9969(01)00121-1).
- Mahony J, McDonnell B, Casey E, van Sinderen D. 2016. Phage-host interactions of cheese-making lactic acid bacteria. *Annu Rev Food Sci Technol* 7:267–285. <https://doi.org/10.1146/annurev-food-041715-033322>.
- Labrie SJ, Samson JE, Moineau S. 2010. Bacteriophage resistance mechanisms. *Nat Rev Microbiol* 8:317–327. <https://doi.org/10.1038/nrmicro2315>.
- Mahony J, van Sinderen D. 2015. Novel strategies to prevent or exploit phages in fermentations, insights from phage-host interactions. *Curr Opin Biotechnol* 32:8–13. <https://doi.org/10.1016/j.copbio.2014.09.006>.
- Guglielmotti DM, Mercanti DJ, Reinheimer JA, Quiberoni AL. 2012. Review: efficiency of physical and chemical treatments on the inactivation of dairy bacteriophages. *Front Microbiol* 2:282. <https://doi.org/10.3389/fmicb.2011.00282>.
- Derx PMF, Janzen T, Sorensen KI, Christensen JE, Stuer-Lauridsen B, Johansen E. 2014. The art of strain improvement of industrial lactic acid bacteria without the use of recombinant DNA technology. *Microb Cell Fact* 13 Suppl 1:S5. <https://doi.org/10.1186/1475-2859-13-S1-S5>.
- Binetti AG, Bailo NB, Reinheimer JA. 2007. Spontaneous phage-resistant mutants of *Streptococcus thermophilus*: isolation and technological characteristics. *Int Dairy J* 17:343–349. <https://doi.org/10.1016/j.idairyj.2006.05.002>.
- Mills S, Coffey A, McAuliffe OE, Meijer WC, Hafkamp B, Ross RP. 2007.

- Efficient method for generation of bacteriophage insensitive mutants of *Streptococcus thermophilus* yoghurt and mozzarella strains. *J Microbiol Methods* 70:159–164. <https://doi.org/10.1016/j.mimet.2007.04.006>.
10. Rodríguez C, Van Der Meulen R, Vaningelgem F, Font De Valdez G, Raya R, De Vuyst L, Mozzi F. 2008. Sensitivity of capsular-producing *Streptococcus thermophilus* strains to bacteriophage adsorption. *Lett Appl Microbiol* 46:462–468. <https://doi.org/10.1111/j.1472-765X.2008.02341.x>.
  11. Lucchini S, Sidoti J, Brüssow H. 2000. Broad-range bacteriophage resistance in *Streptococcus thermophilus* by insertional mutagenesis. *Virology* 275:267–277. <https://doi.org/10.1006/viro.2000.0499>.
  12. McDonnell B, Mahony J, Hanemaaijer L, Kouwen TRHM, van Sinderen D. 2018. Generation of bacteriophage-insensitive mutants of *Streptococcus thermophilus* via an antisense RNA CRISPR-Cas silencing approach. *Appl Environ Microbiol* 84:e01733-17. <https://doi.org/10.1128/AEM.01733-1>.
  13. Binetti AG, Suárez VB, Tailliez P, Reinheimer JA. 2007. Characterization of spontaneous phage-resistant variants of *Streptococcus thermophilus* by randomly amplified polymorphic DNA analysis and identification of phage-resistance mechanisms. *Int Dairy J* 17:1115–1122. <https://doi.org/10.1016/j.idairyj.2007.01.007>.
  14. Mills S, Griffin C, Coffey A, Meijer WC, Hafkamp B, Ross RP. 2010. CRISPR analysis of bacteriophage-insensitive mutants (BIMs) of industrial *Streptococcus thermophilus*—implications for starter design. *J Appl Microbiol* 108:945–955. <https://doi.org/10.1111/j.1365-2672.2009.04486.x>.
  15. Larbi D, Decaris B, Simonet J-M. 1992. Different bacteriophage resistance mechanisms in *Streptococcus salivarius* subsp. *thermophilus*. *J Dairy Res* 59:349. <https://doi.org/10.1017/S0022029900030624>.
  16. Ali Y, Koberg S, Heßner S, Sun X, Rabe B, Back A, Neve H, Heller KJ. 2014. Temperate *Streptococcus thermophilus* phages expressing superinfection exclusion proteins of the Ltp type. *Front Microbiol* 5:98. <https://doi.org/10.3389/fmicb.2014.00098>.
  17. Dupuis M-E, Villion M, Magadán AH, Moineau S. 2013. CRISPR-Cas and restriction-modification systems are compatible and increase phage resistance. *Nat Commun* 4:2087. <https://doi.org/10.1038/ncomms3087>.
  18. Deveau H, Barrangou R, Garneau JE, Labonté J, Fremaux C, Boyaval P, Romero DA, Horvath P, Moineau S. 2008. Phage response to CRISPR-encoded resistance in *Streptococcus thermophilus*. *J Bacteriol* 190:1390–1400. <https://doi.org/10.1128/JB.01412-07>.
  19. Barrangou R, Fremaux C, Deveau H, Richards M, Boyaval P, Moineau S, Romero DA, Horvath P. 2007. CRISPR provides acquired resistance against viruses in prokaryotes. *Science* 315:1709–1712. <https://doi.org/10.1126/science.1138140>.
  20. Paez-Espino D, Morovic W, Sun CL, Thomas BC, Ueda KI, Stahl B, Barrangou R, Banfield JF. 2013. Strong bias in the bacterial CRISPR elements that confer immunity to phage. *Nat Commun* 4:1430–1437. <https://doi.org/10.1038/ncomms2440>.
  21. Paez-Espino D, Sharon I, Morovic W, Stahl B, Thomas BC, Barrangou R, Banfield JF. 2015. CRISPR immunity drives rapid phage genome evolution in *Streptococcus thermophilus*. *mBio* 6:e00262-15. <https://doi.org/10.1128/mBio.00262-15>.
  22. McGrath S, Seegers JFML, Fitzgerald GF, Grath SMC, van Sinderen D. 1999. Molecular characterization of a phage-encoded resistance system in *Lactococcus lactis*. *Appl Environ Microbiol* 65:1891–1899.
  23. Bondy-Denomy J, Pawluk A, Maxwell KL, Davidson AR. 2013. Bacteriophage genes that inactivate the CRISPR/Cas bacterial immune system. *Nature* 493:429–432. <https://doi.org/10.1038/nature11723>.
  24. Bondy-Denomy J, Garcia B, Strum S, Mingjian D, Rollins MF, Hidalgo-Reyes Y, Wiedenheft B, Maxwell KL, Davidson AR. 2015. Multiple mechanisms for CRISPR-Cas inhibition by anti-CRISPR proteins. *Nature* 526:136–139. <https://doi.org/10.1038/nature15254>.
  25. Viscardi M, Capparelli R, Di Matteo R, Carminati D, Giraffa G, Iannelli D. 2003. Selection of bacteriophage-resistant mutants of *Streptococcus thermophilus*. *J Microbiol Methods* 55:109–119. [https://doi.org/10.1016/S0167-7012\(03\)00146-5](https://doi.org/10.1016/S0167-7012(03)00146-5).
  26. Seed KD. 2015. Battling phages: how bacteria defend against viral attack. *PLoS Pathog* 11:e1004847. <https://doi.org/10.1371/journal.ppat.1004847>.
  27. Chapot-Chartier M-P, Kulakauskas S. 2014. Cell wall structure and function in lactic acid bacteria. *Microb Cell Fact* 13:59. <https://doi.org/10.1186/1475-2859-13-S1-59>.
  28. Zeidan AA, Poulsen VK, Janzen T, Buldo P, Derx PMF, Oregaard G, Neves AR. 2017. Polysaccharide production by lactic acid bacteria: from genes to industrial applications. *FEMS Microbiol Rev* 41:5168–5200. <https://doi.org/10.1093/femsre/fux017>.
  29. Chapot-Chartier M-P, Vinogradov E, Sadovskaya I, Andre G, Mistou M-Y, Trieu-Cuot P, Furlan S, Bidnenko E, Courtin P, Pêchoux C, Hols P, Dufréne YF, Kulakauskas S. 2010. Cell surface of *Lactococcus lactis* is covered by a protective polysaccharide pellicle. *J Biol Chem* 285:10464–10471. <https://doi.org/10.1074/jbc.M109.082958>.
  30. Mistou MY, Sutcliffe IC, Van Sorge NM. 2016. Bacterial glycobiology: rhamnose-containing cell wall polysaccharides in Gram-positive bacteria. *FEMS Microbiol Rev* 40:464–479. <https://doi.org/10.1093/femsre/fuw006>.
  31. Brown S, Santa Maria JP, Jr, Walker S. 2013. Wall teichoic acids of Gram-positive bacteria. *Annu Rev Microbiol* 67:313–336. <https://doi.org/10.1146/annurev-micro-092412-155620>.
  32. Reichmann NT, Gründling A. 2011. Location, synthesis and function of glycolipids and polyglycerolphosphate lipoteichoic acid in Gram-positive bacteria of the phylum *Firmicutes*. *FEMS Microbiol Lett* 319:97–105. <https://doi.org/10.1111/j.1574-6968.2011.02260.x>.
  33. Mahony J, van Sinderen D. 2012. Structural aspects of the interaction of dairy phages with their host bacteria. *Viruses* 4:1410–1424. <https://doi.org/10.3390/v4091410>.
  34. Ainsworth S, Sadovskaya I, Vinogradov E, Courtin P, Guerardel Y, Mahony J, Grard T, Cambillau C, Chapot-Chartier MP, van Sinderen D. 2014. Differences in lactococcal cell wall polysaccharide structure are major determining factors in bacteriophage sensitivity. *mBio* 5:e00880-14. <https://doi.org/10.1128/mBio.00880-14>.
  35. Bebeacqua C, Tremblay D, Farenc C, Chapot-Chartier M-P, Sadovskaya I, van Heel M, Veessler D, Moineau S, Cambillau C. 2013. Structure, adsorption to host, and infection mechanism of virulent lactococcal phage p2. *J Virol* 87:12302–12312. <https://doi.org/10.1128/JVI.02033-13>.
  36. Collins B, Bebeacqua C, Mahony J, Blangy S, Douillard FP, Veessler D, Cambillau C, van Sinderen D. 2013. Structure and functional analysis of the host recognition device of lactococcal phage Tuc2009. *J Virol* 87:8429–8440. <https://doi.org/10.1128/JVI.00907-13>.
  37. Mahony J, Kot W, Murphy J, Ainsworth S, Neve H, Hansen LH, Heller KJ, Sørensen SJ, Hammer K, Cambillau C, Vogensen FK, van Sinderen D. 2013. Investigation of the relationship between lactococcal host cell wall polysaccharide genotype and 936 phage receptor binding protein phylogeny. *Appl Environ Microbiol* 79:4385–4392. <https://doi.org/10.1128/AEM.00653-13>.
  38. Bebeacqua C, Bron P, Lai L, Vegge CS, Brøndsted L, Spinelli S, Campanacci V, Veessler D, Van Heel M, Cambillau C. 2010. Structure and molecular assignment of lactococcal phage TP901-1 baseplate. *J Biol Chem* 285:39079–39086. <https://doi.org/10.1074/jbc.M110.175646>.
  39. Spinelli S, Campanacci V, Blangy S, Moineau S, Tegoni M, Cambillau C. 2006. Modular structure of the receptor binding proteins of *Lactococcus lactis* phages. The RBP structure of the temperate phage TP901-1. *J Biol Chem* 281:14256–14262.
  40. Lubbers MW, Waterfield NR, Beresford TPJ, Le Page RWF, Jarvis WA. 1995. Sequencing and analysis of the prolate-headed lactococcal bacteriophage c2 genome and identification of the structural genes. *Appl Environ Microbiol* 61:4348–4356.
  41. Geller BL, Ivey RG, Trempey JE, Hettinger-Smith B. 1993. Cloning of a chromosomal gene required for phage infection of *Lactococcus lactis* subsp. *lactis* c2. *J Bacteriol* 175:5510–5519. <https://doi.org/10.1128/jb.175.17.5510-5519.1993>.
  42. Räsänen L, Schubert K, Jaakonsaari T, Alatossava T. 2004. Characterization of lipoteichoic acids as *Lactobacillus delbrueckii* phage receptor components. *J Bacteriol* 186:5529–5532. <https://doi.org/10.1128/JB.186.16.5529-5532.2004>.
  43. Räsänen L, Draing C, Pfitzenmaier M, Schubert K, Jaakonsaari T, Von Aulock S, Hartung T, Alatossava T. 2007. Molecular interaction between lipoteichoic acids and *Lactobacillus delbrueckii* phages depends on D-alanyl and  $\alpha$ -glucose substitution of poly(glycerophosphate) backbones. *J Bacteriol* 189:4135–4140. <https://doi.org/10.1128/JB.00078-07>.
  44. Munsch-Alatossava P, Alatossava T. 2013. The extracellular phage-host interactions involved in the bacteriophage LL-H infection of *Lactobacillus delbrueckii* subsp. *lactis* ATCC 15808. *Front Microbiol* 4:408. <https://doi.org/10.3389/fmicb.2013.00408>.
  45. Szymczak P, Janzen T, Neves AR, Kot W, Hansen LH, Lametsch R, Neve H, Franz CMAP, Vogensen FK. 2017. Novel variants of *Streptococcus thermophilus* bacteriophages are indicative of genetic recombination among phages from different bacterial species. *Appl Environ Microbiol* 83:e02748-16. <https://doi.org/10.1128/AEM.02748-16>.
  46. McDonnell B, Mahony J, Hanemaaijer L, Neve H, Noben J-P, Lugli GA, Ventura M, Kouwen TR, van Sinderen D. 2017. Global survey and genome exploration of bacteriophages infecting the lactic acid bacterium

- Streptococcus thermophilus*. Front Microbiol 8:1754. <https://doi.org/10.3389/fmicb.2017.01754>.
47. McDonnell B, Mahony J, Neve H, Hanemaaijer L, Noben J-P, Kouwen T, van Sinderen D. 2016. Identification and analysis of a novel group of bacteriophages infecting the lactic acid bacterium *Streptococcus thermophilus*. Appl Environ Microbiol 82:e00835-16. <https://doi.org/10.1128/AEM.00835-16>.
  48. Mahony J, van Sinderen D. 2014. Current taxonomy of phages infecting lactic acid bacteria. Front Microbiol 5:7. <https://doi.org/10.3389/fmicb.2014.00007>.
  49. Quiberoni A, Stiefel JI, Reinheimer JA. 2000. Characterization of phage receptors in *Streptococcus thermophilus* using purified cell walls obtained by a simple protocol. J Appl Microbiol 89:1059–1065. <https://doi.org/10.1046/j.1365-2672.2000.01214.x>.
  50. Horvath P, Romero DA, Coûté-Monvoisin A-C, Richards M, Deveau H, Moineau S, Boyaval P, Fremaux C, Barrangou R. 2008. Diversity, activity, and evolution of CRISPR loci in *Streptococcus thermophilus*. J Bacteriol 190:1401–1412. <https://doi.org/10.1128/JB.01415-07>.
  51. Layec S, Gérard J, Legué V, Chapot-Chartier M-P, Courtin P, Borges F, Decaris B, Leblond-Bourget N. 2009. The CHAP domain of Cse functions as an endopeptidase that acts at mature septa to promote *Streptococcus thermophilus* cell separation. Mol Microbiol 71:1205–1217. <https://doi.org/10.1111/j.1365-2958.2009.06595.x>.
  52. Formstone A, Carballido-López R, Noirot P, Errington J, Scheffers D-J. 2008. Localization and interactions of teichoic acid synthetic enzymes in *Bacillus subtilis*. J Bacteriol 190:1812–1821. <https://doi.org/10.1128/JB.01394-07>.
  53. Atilano ML, Pereira PM, Yates J, Reed P, Veiga H, Pinho MG, Filipe SR. 2010. Teichoic acids are temporal and spatial regulators of peptidoglycan cross-linking in *Staphylococcus aureus*. Proc Natl Acad Sci U S A 107:18991–18996. <https://doi.org/10.1073/pnas.1004304107>.
  54. Schlag M, Biswas R, Krismer B, Kohler T, Zoll S, Yu W, Schwarz H, Peschel A, Götz F. 2010. Role of staphylococcal wall teichoic acid in targeting the major autolysin Atl. Mol Microbiol 75:864–873. <https://doi.org/10.1111/j.1365-2958.2009.07007.x>.
  55. Pachekrepapol U, Lucey JA, Gong Y, Naran R, Azadi P. 2017. Characterization of the chemical structures and physical properties of exopolysaccharides produced by various *Streptococcus thermophilus* strains. J Dairy Sci 100:3424–3435. <https://doi.org/10.3168/jds.2016-12125>.
  56. Delcour J, Ferain T, Deghorain M, Palumbo E, Hols P. 1999. The biosynthesis and functionality of the cell-wall of lactic acid bacteria. Antonie Van Leeuwenhoek 76:159–184. <https://doi.org/10.1023/A:1002089722581>.
  57. Johansen E. 2003. Challenges when transferring technology from *Lactococcus* laboratory strains to industrial strains. Genet Mol Res 2:112–116.
  58. Hols P, Hancy F, Fontaine L, Grossiord B, Prozzi D, Leblond-Bourget N, Decaris B, Bolotin A, Delorme C, Ehrlich SD, Guédon E, Monnet V, Renault P, Kleerebezem M. 2005. New insights in the molecular biology and physiology of *Streptococcus thermophilus* revealed by comparative genomics. FEMS Microbiol Rev 29:435–463. <https://doi.org/10.1016/j.fmrre.2005.04.008>.
  59. Bebeacua C, Lai L, Vegge CS, Brøndsted L, van Heel M, Velesler D, Cambillau C. 2013. Visualizing a complete *Siphoviridae* member by single-particle electron microscopy: the structure of lactococcal phage TP901-1. J Virol 87:1061–1068. <https://doi.org/10.1128/JVI.02836-12>.
  60. Filipe SR, Tomasz A. 2000. Inhibition of the expression of penicillin resistance in *Streptococcus pneumoniae* by inactivation of cell wall muropetide branching genes. Proc Natl Acad Sci U S A 97:4891–4896. <https://doi.org/10.1073/pnas.080067697>.
  61. Garcia-Bustos JF, Chait BT, Tomasz A. 1988. Altered peptidoglycan structure in a pneumococcal transformant resistant to penicillin. J Bacteriol 170:2143–2147. <https://doi.org/10.1128/jb.170.5.2143-2147.1988>.
  62. Kropinski AM, Mazzocco A, Waddell TE, Lingohr E, Johnson RP. 2009. Enumeration of bacteriophages by double agar overlay plaque assay. Methods Mol Biol 501:69–76. [https://doi.org/10.1007/978-1-60327-164-6\\_7](https://doi.org/10.1007/978-1-60327-164-6_7).
  63. Henriques MX, Catalão MJ, Figueiredo J, Gomes JP, Filipe SR. 2013. Construction of improved tools for protein localization studies in *Streptococcus pneumoniae*. PLoS One 8:e55049. <https://doi.org/10.1371/journal.pone.0055049>.
  64. Dupont K, Vogensen FK, Neve H, Bresciani J, Josephsen J. 2004. Identification of the receptor-binding protein in 936-species lactococcal bacteriophages. Appl Environ Microbiol 70:5818–5824. <https://doi.org/10.1128/AEM.70.10.5818-5824.2004>.
  65. Abràmoff MD, Hospitals I, Magalhães PJ, Abràmoff M. 2004. Image processing with ImageJ. Biophotonics Int 11:36–42.
  66. Monteiro JM, Fernandes PB, Vaz F, Pereira AR, Tavares AC, Ferreira MT, Pereira PM, Veiga H, Kuru E, VanNieuwenhze MS, Brun YV, Filipe SR, Pinho MG. 2015. Cell shape dynamics during the staphylococcal cell cycles. Nat Commun 6:8055. <https://doi.org/10.1038/ncomms9055>.
  67. Carvalho F, Atilano ML, Pombinho R, Covas G, Gallo RL, Filipe SR, Sousa S, Cabanes D. 2015. L-Rhamnosylation of *Listeria monocytogenes* wall teichoic acids promotes resistance to antimicrobial peptides by delaying interaction with the membrane. PLoS Pathog 11:e1004919. <https://doi.org/10.1371/journal.ppat.1004919>.
  68. Brettin T, Davis JJ, Disz T, Edwards Ra, Gerdes S, Olsen GJ, Olson R, Overbeek R, Parrello B, Pusch GD, Shukla M, Thomason JA, Stevens R, Vonstein V, Wattam AR, Xia F. 2015. RASTtk: a modular and extensible implementation of the RAST algorithm for building custom annotation pipelines and annotating batches of genomes. Sci Rep 5:8365. <https://doi.org/10.1038/srep08365>.